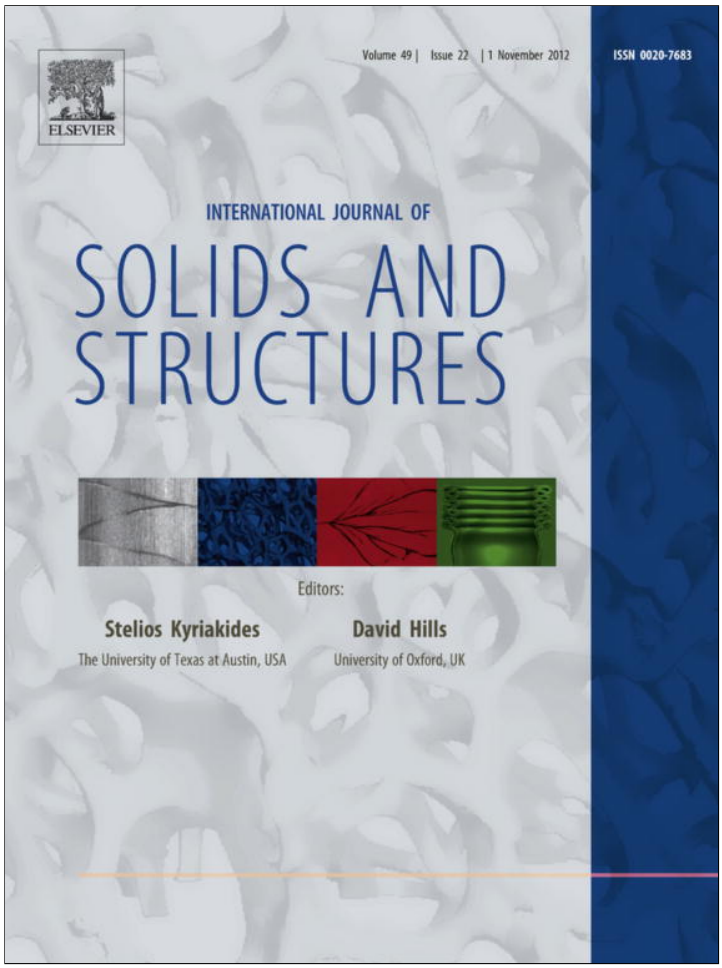

International Journal of Solids and Structures 49 (2012) 3089–3099

Contents lists available at SciVerse ScienceDirect

International Journal of Solids and Structures

journal homepage: www.elsevier.com/locate/ijsolstr

Elastic behaviour of a regular lattice for meso-scale modelling of solids

Andrey P. Jivkov [a,b,*], John R. Yates [b]

[a] Research Centre for Radwaste and Decommissioning, Dalton Nuclear Institute, The University of Manchester, Manchester M13 9PL, UK
[b] Modelling and Simulation Centre, Dalton Nuclear Institute, The University of Manchester, Manchester M13 9PL, UK

ARTICLE INFO

Article history:
Received 24 December 2011
Received in revised form 10 May 2012
Available online 29 June 2012

Keywords:
Microstructure
Meso-scale
Regular structure
Site-bond model
Elastic properties
Constitutive behaviour

ABSTRACT

A modelling strategy is proposed to link the meso-scale mechanical response of a solid material to the macroscopic material behaviour. The model is based on a regular lattice of truncated octahedral cells, with sites at the cell centres linked by two sets of bonds. The relationship between the macroscopic elastic behaviour of the model and the elastic properties of the bonds is studied numerically. The results demonstrate that, in contrast to previously proposed lattice arrangements, any elastic properties of metallic or cementitious materials can be obtained by appropriate selection of the axial and the shear stiffness of the bonds. Discussion of the modelling approach includes the potential of the site-bond model to simulate the evolution of damage driven not only by mechanical deformation but also by processes that involve the interaction of different mechanisms.

1. Introduction

Current modelling and simulation practices for engineering analyses are based on continuum descriptions of material responses to external driving forces. These may be stresses due to deformation gradients; heat fluxes due to temperature gradients; fluid flows in porous media due to pressure gradients; diffusion of chemical species due to concentration gradients; and electric current due to potential gradients. The basis of the continuum approach is to relate the responses to the driving forces by governing differential equations and formulate appropriate boundary value problems that can be solved with any number of numerical schemes, most commonly the finite element method.

A key feature of the continuum approach is the definition of constitutive laws to link the driving forces for particular phenomena with their evolution. Generally, these laws are phenomenological, based on accumulated knowledge from macroscopic experiments. However, the continuum approach may break down in the presence of discontinuities, such as existing or emerging voids or micro-cracks which can grow, interact and coalesce. Thanks to advances in experimental materials science our understanding of the microscopic mechanisms responsible for the creation and growth of discontinuities is improving continually. For example, the stress driven motion of dislocations in metallic materials can lead to de-cohesion (Argon et al., 1975; Xu and Needleman, 1993) or rupture (Curry and Knott, 1979; Chen and Wang, 1992) of second-phase particles. Similarly, localised cavitations, nucleation of micro-cracks, enlargement or shrinkage of existing voids in man-made or natural materials can occur due to diffusion of species (Chen and Argon, 1981; Cocks and Ashby, 1982), electrochemical processes (Lo et al., 2009; Jain et al., 2010), and even bacterial effects (Taylor and Jaffe, 1990; Lo et al., 2009).

Advances in engineering design and assessment will require increasing accuracy in accounting for the effects of microscopic failures on, for example, macroscopic deformation behaviour; thermal conductivity; hydraulic permeability; diffusivity; or electric conductivity. One important area is the deformation behaviour of metallic materials in the fracture process zone in the vicinity of a macroscopic crack, which is relevant to the energy, automotive, aerospace and rail industries. This may be coupled with thermal and corrosion effects on the formation and growth of microscopic flaws. Another important area is the deformation and conductive behaviour of porous quasi-brittle materials, such as cements, concretes, geological materials, nuclear graphite, and human bone. These may also be coupled with thermal, corrosion and bacterial effects. Micro-failures may also lead to changes in electric conductivity, which is an important problem for the power generation and transmission, and electronic industries.

All these industries will continue to use continuum approaches to modelling materials and components performance for the foreseeable future. This is dictated by the vast intellectual effort invested in the development of its theoretical basis, computational implementation and developing engineering expertise. One practical constraint to the continuum approach is the derivation of the

* Corresponding author at: Research Centre for Radwaste and Decommissioning, Dalton Nuclear Institute, The University of Manchester, Manchester M13 9PL, UK. Tel.: +44 0 161 275 0402; fax: +44 0 161 200 3723.
E-mail addresses: andrey.jivkov@manchester.ac.uk (A.P. Jivkov), john.r.yates@manchester.ac.uk (J.R. Yates).

0020-7683/$ - see front matter © 2012 Elsevier Ltd. All rights reserved.
http://dx.doi.org/10.1016/j.ijsolstr.2012.06.010

necessary multi-variable phenomenological constitutive laws. Such derivation entails unaffordable experimental programmes.

The basis of the work reported in this paper is the premise that macroscopic constitutive laws may be derived from observing and modelling the physical processes operating at shorter length scales. Such macroscopic constitutive laws will therefore be mechanism-based as opposed to phenomenological. The immediate aim is to formulate a framework for modelling solid materials that allows scientists and engineers to bridge the gap between knowledge of microscopic mechanisms of deformation and failure, and the macroscopic material responses.

The key element to the treatment of microscopic failure mechanisms, which unifies all the cases described above, is the presence of microscopic defects with random spatial and size distributions. These can be micro-cracks, voids, pores, second-phase particles, and such like, which act as micro-failure initiators. The continuum approach is capable of dealing with such defects only if they are pre-defined in size and spatial arrangements. For example, fracture mechanics modelling requires the definition of cracked geometries and ideally the knowledge of crack extension paths if crack advance is to be analysed. Some recent methods, such as the extended finite element method (Sukumar et al., 2000), allow for modelling arbitrary crack paths, according to prescribed macroscopic criteria. However, the interaction and the coalescence of multiple cracks cannot be addressed with these methods without bringing in additional constitutive assumptions. Further the continuum approach is inherently incapable of dealing with initiation phases of failure. The nucleation of micro-failures, their growth, interaction and coalescence are of fundamental importance in the assessment of macroscopic behaviour and the derivation of mechanism-based continuum constitutive laws.

Progress in using the mechanistic understanding of microscopic phenomena for macroscopic constitutive laws or failure predictions has been made in the area of fracture mechanics of metallic materials. For the case of ductile fracture, the understanding of the void growth and coalescence mechanism has led to a number of ductile-damage models (Rice and Tracey, 1969; Gurson, 1977; Tvergaard and Needleman, 1984; Thomason, 1985; Rousselier, 1987), where material damage due to void enlargement is represented by pressure-dependent terms in the constitutive material response. Thus, the void network is "smeared" in the continuum, which does not allow for proper treatment of their interaction and coalescence. Additional phenomenological assumptions have to be made to account for these processes. For the case of cleavage fracture, the understanding of the role of plastic strain, principal stress and stress triaxiality on the rupture of second-phase particles has lead to a number of probabilistic models for brittle failure (Beremin et al., 1983; Mudry, 1987; Ruggieri and Dodds, 1996; Bordet et al., 2005). However, the common assumption for all these models is that the global failure is a weakest-link event; the microscopic failure events are assumed to be isolated and independent. While this may be a good approximation for cases with a very low density of micro-failures, at very low plastic strain levels for instance, the interactions between micro-failures becomes sufficiently influential at higher micro-failure densities to invalidate the weakest-link statistics (Jivkov et al., 2011).

The constitutive laws for the behaviour of porous quasi-brittle materials, concretes, rocks and clays, are based on a number of cohesion and pressure dependent brittle- or ductile-damage models. These rely on curve fitting to macroscopic experimental data to identify and calibrate the parameters (de Borst, 2002; Jing, 2003; Hofstetter and Meschke, 2011). Failure analysis of such materials is generally based on weakest-link statistics, similar to the cleavage failure of metals, although its validity has been repeatedly questioned, particularly on the grounds of failing to account for interaction and coalescence of micro-failures (Bazant and Pang, 2007). To date, there is no general framework for studying the effects of micro-failures on the thermal conductivity, hydraulic conductivity or diffusivity of these materials.

These observations suggest that there is advantage in creating a material representation that allows for micro-failure initiation, growth, interaction and coalescence and yet is suitable for analysing changes in the macroscopic properties. A promising approach for constructing such a representation is use of the discrete particle methods. The origin of these methods can be found in fluid mechanics, with smoothed particle hydrodynamics being a notable modern flavour (Monaghan, 2005). Recent developments for solid mechanics are the smoothed particle applied mechanics (Hoover and Hoover, 2001) and the peridynamics (Silling, 2000). These methods, however, have been developed from a continuum material perspective; without explicit account being taken of the underlying microstructure and micro-mechanisms of failure. This makes it difficult to incorporate some of the complexity, particularly in terms of coupled mechanisms, that may be involved in the nucleation and growth of micro-failures. Furthermore, investigating the influence of micro-failures on other macroscopic properties, such as permeability and electrical conductivity, becomes intractable without a sound mechanistic framework. Models developed from a microstructure and micro-mechanistic basis would be more advantageous in this respect.

Material representations that can incorporate variable behaviours at a microstructural scale can be constructed from lattices of space-filling polyhedra. Each polyhedron is an individual cell that represents a particular microstructural feature; usually a grain, but it may be the environs of the largest defects. Computationally, the solid is represented by a framework of linear structural elements with nodes at the centres of the cells and elements linking neighbouring nodes. The macroscopic mechanical behaviour of the solid is obtained by the assignment of deformation and failure properties to the elements. *The basic prerequisite for such models is that they must be able to generate the macroscopic elastic properties of the material.* This requirement should be met before any failure characteristics are assigned for studying micro-cracking effects on the macroscopic mechanical behaviour.

The lattice approach has been used previously for modelling cementitious materials. Early works, based on 2D regular hexagonal lattice (Schlangen and van Mier, 1992; Chang et al., 2002), provide a good illustration that the non-linearity in the macroscopic stress–strain curve for such materials is an emergent property from the underlying micro-cracking events. It has been analytically derived, however, that this lattice cannot be used for materials with Poisson's ratio larger than 0.25 in plane strain and 0.33 in plane stress (Griffiths and Mustoe, 2001). Moreover, the number of cases where a 2D representation of a solid is appropriate is limited. Micro-crack growth and coalescence is a truly three-dimensional phenomenon. A 3D model has been proposed based on the simplest regular lattice with cubic cells (Schlangen, 2008). One problem with this lattice is that it is not physically realistic in terms of the shape of the represented grains; the shapes of the formed grain boundaries; or the coordination with neighbouring grains. Moreover, this lattice is unable to provide a linear elastic response with an appropriate elastic modulus and Poisson's ratio. Two more complex 3D lattices, based on face-centred cubic and hexagonal closely-packed arrangements have also been analysed (Wang and Mora, 2008). It has been shown that these lattices can represent an isotropic homogeneous linear elastic material only when the Poisson's ratio equals zero, which is precisely the result for a cubic lattice. It is worth mentioning that modelling with irregular lattices, such as those formed from Delaunay triangulations of 3D material volumes, has also been suggested (Cusatis et al., 2006). Such lattices, however, are specific to the material domains being represented and analysis of the link between the

elastic properties of the elements and the elastic behaviour of the assembly is not straightforward.

A lattice built from truncated octahedrons has been used in studies of intergranular stress corrosion cracking (Jivkov et al., 2006). However, the wider capabilities of this lattice model have not been addressed; in particular its ability to reproduce any macroscopic elastic behaviour of practical interest. In this work we demonstrate that this lattice provides a useful and physically realistic representation of a solid material at a meso-scale, the scale dictated by the microscopic mechanisms of failure. We show that the computational model of nodes and elements corresponding to the lattice, which we call the site-bond model, can be tuned to represent any pre-defined macroscopic elastic behaviour. An attraction of the proposed model is the ability to vary independently the elastic properties of the two types of bonds present in the lattice. Our demonstration is based on numerical experiments. Finally, we discuss the potential of such a discrete model to derive constitutive relationships for continuum models from the knowledge of underlying microscopic mechanisms.

2. Solids at meso-scale

We consider the meso-scale to be a length scale relevant to a particular mechanism of microscopic failure or micro-crack formation. The mechanism is related to the presence of micro-defects which act as failure initiators. In porous quasi-brittle materials micro-defects are present in the form of pores residing at the interfaces between solid-phase grains. The mechanical deformation of the material leads to failure of such interfaces forming micro-cracks which may grow, interact and coalesce. The meso-scale for these materials is dictated naturally by the size of the solid-phase grains. In metallic materials micro-defects are present in the form of second-phase particles, typically harder than the surrounding matrix. The mechanical deformation of the material may cause rupture of such particles, resulting in micro-crack nucleation, or de-cohesion of particles from the matrix, resulting in void formation. The meso-scale in such cases is dictated by the spacing between characteristic, sufficiently large, initiators. If these initiators are found predominantly at the grain boundaries, the meso-scale would be determined by the size of the crystals in the polycrystalline assembly. Otherwise, one can reformulate the notion of a grain so that it stands for a domain free of characteristic initiators, whilst the initiators are allowed to reside at the domain boundaries. This position allows the development of a common approach to a wide class of engineering and geological materials.

In our method, a physical region is tessellated into cells free of micro-defects. The failure initiators are allowed to be distributed on the interfaces between the cells. As we aim to construct a simple regular model of the microstructure, it is important to select the cell shape and coordination which is a reasonable representation of real materials. Tessellating a domain of a real material into cells with micro-defects residing at interfaces would produce a Voronoi diagram of the point set determined by the grain, or reformulated grain, centres. Monte Carlo studies with 3D Voronoi tessellations of space (Kumar et al., 1992) have shown that: the average number of cell faces (F), or the average cell coordination, is 15.54; the average number of cell edges (E) is 40.63; the average number of cell vertices (V) is 27.09; and the mean number of edges per face (S) is 5.23. This provides an insight into the selection of a regular cell shape. Four geometric solids can fill space compactly using a single solid cell. These are: the cube with $F = 6$, $E = 12$, $V = 8$, $S = 4$; the regular hexagonal prism with $F = 8$, $E = 18$, $V = 12$, $S = 4.5$; the rhombic dodecahedron, a solid bounded by 12 equal rhombuses, with $F = 12$, $E = 24$, $V = 14$, $S = 4$; and the truncated octahedron, a solid bounded by six equal squares and eight equal regular hexagons, with $F = 14$, $E = 36$, $V = 24$, $S = 5.14$. This suggests that the best choice for a regular representation of the microstructure is the truncated octahedron. Fig. 1 shows an illustration of this solid, as well as an assembly of cells in a 3D lattice.

The next step of model abstraction is to consider the cell centres as geometric points or sites, with neighbouring sites connected by one-dimensional links or bonds. The deformation behaviour of a bond has to account for all possible relative deformations between the two adjacent cells. In other words, the bond must be able to describe all relative displacements and rotations between the coordinated sites. Furthermore, the bonds intersect the interfaces between cells where micro-defects may reside. Correspondingly, the bonds may be attributed failure properties dictated by a particular failure micro-mechanism.

A single site-bond model, as described, may well be sufficient to investigate macroscopic responses that are only governed by micro-failures mechanisms driven by the deformation of the material. In cases of micro-failure mechanisms driven by other phenomena, such as electrochemical or bacterial corrosion, or diffusion, or investigations of other macroscopic properties, such as hydraulic permeability, or species diffusivity, the proposed site-bond model can be complemented by a dual site-bond model. In such cases, the primary sites characterise the solid phase, and the secondary sites characterise an additional phase, such as a system of voids or pores. The sites of the secondary model are the centres of the bonds in the primary model and the bonds of the secondary model link adjacent interfaces of the primary model. Examples of this methodology are discussed in more detail in Section 5.

The critical point for this concept to be accepted is whether the site-bond model of the solid phase is able to reproduce any desired macroscopic elastic response. In the next two sections we will describe a computational implementation of the site-bond model and will demonstrate that the model is capable of reproducing any required macroscopic elastic properties of practical interest.

3. Model and method

The construction of the site-bond model begins with the seeding of sites. This uses a mapping from integer triplets (i,j,k) into the physical space. Only triplets with three even indices (even triplets) and three odd indices (odd triplets) are mapped into sites. For the mapping, we assume equal spacing between the sites of the assembly in the three principal directions, i.e. the directions normal to the square faces of the solid cell in Fig. 1, and denote this spacing by L. This assumption yields a site-bond model corresponding to the cell assembly of Fig. 1, with L giving the size of the unit cell in any of the principal directions. Generally, unequal spacing in the principal directions could be considered if one wishes to obtain grains with distorted shapes to mimic texture, for example. This possibility is beyond the scope of the current work. With equal spacing in the principal directions, L, the sites of the assembly are seeded at points with coordinates $(i\,L/2, j\,L/2, k\,L/2)$ in the physical space. The sites mapped from even triplets and from odd triplets form two sets of sites in the physical space. The sites from each set are connected by bonds to the neighbouring six sites of the same set and to the neighbouring eight sites of the other set.

Fig. 2 illustrates the site-bond assembly so formed. The sites are depicted by small spheres, and the bonds by cylindrical links with two different colours. The bonds connecting sites belonging to the same set are denoted by B_1. They have length $L_1 = L$ and are normal to the square faces of the cellular representation in Fig. 1. The bonds connecting sites belonging to two different site sets are denoted by B_2. They have length $L_2 = \sqrt{3}L/2$ and are normal to the hexagonal faces of the truncated octahedron.

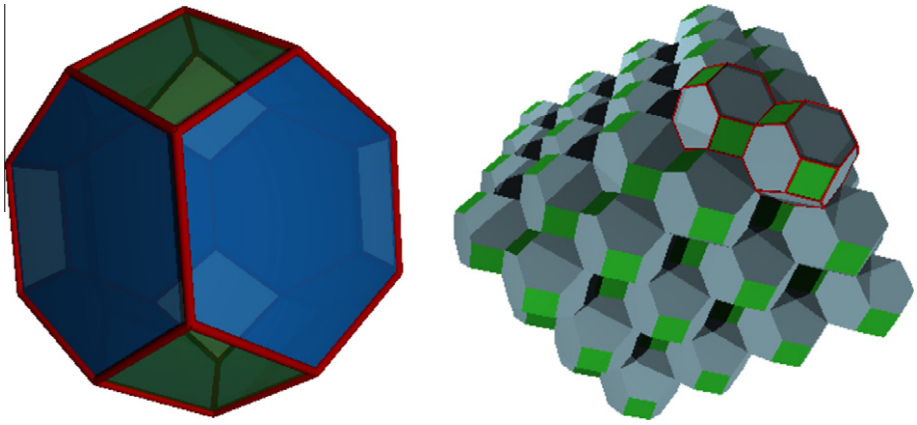

Fig. 1. Unit cell (truncated octahedron) and 3D regular cellular assembly representing material microstructure.

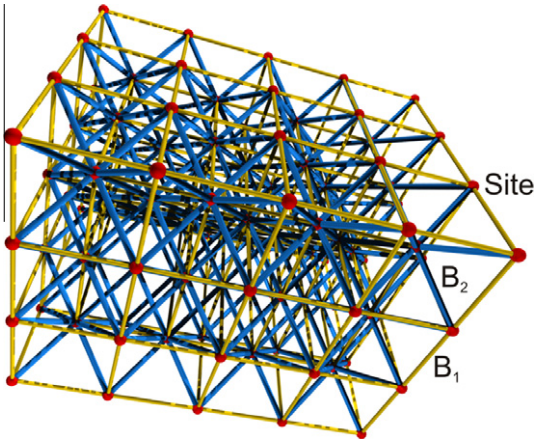

Fig. 2. Site-bond assembly of a 3D solid-phase model.

The bonds of the site-bond assembly are modelled with structural beam elements in order to reflect all possible relative displacements between coordinated sites. Thus the sites have six independent degrees of freedom: three translational and three rotational. Correspondingly, the bonds are capable of transferring axial and shear forces, and torsion and bending moments. This is a principal feature that distinguishes the proposed site-bond model from other discrete methods, such as the discrete element method (Cundall and Hart, 1992).

There are several geometric and material properties associated with the bonds in the assembly. The selection of these properties allows one to model material anisotropy and inhomogeneity. For example, to achieve a particular anisotropic macroscopic response, the bonds in various directions can be assigned different elastic or inelastic deformation and failure behaviours. To represent material inhomogeneity, the bonds belonging to various regions of the assembly can be assigned specific deformation or failure behaviours, common to that region but differing between regions. The latter approach can be used, for example, to represent solid-phase particles of various sizes whilst leaving the simple underlying lattice in place. For this purpose, no failure properties will be attached to the bonds within a region corresponding to a solid-phase grain. Section 5 provides further details on the generality of the model in this respect. We shall now focus on the elastic properties and the geometric characteristics of the bonds needed to produce elastic responses.

Firstly, in this work we assume local material isotropy, hence the bonds should not have any preferential directions for shear and bending. Therefore, the beams are selected to be of circular cross section and the geometric parameters that can be varied are the radii of the cross sections. All beams of length L_1, those connecting sites of one and the same set, are assigned a radius R_1. All beams of length L_2, those connecting sites of the two different sets, are assigned a radius R_2. Secondly, in this work we assume material homogeneity, hence the bonds should not exhibit different elastic behaviour. Therefore, all beams have identical elastic modulus, E_b, and identical modulus of rigidity G_b. The modulus of rigidity dictates the shear and torsional stiffness of the beam, which may affect the macroscopic response of the assembly.

With these settings, the relation between the displacements and rotations, a vector $\mathbf{D}$, and the reaction forces and moments, a vector $\mathbf{F}$, at two coordinated sites p and q is given by a standard symmetric 12×12 beam stiffness matrix, K, so that $\mathbf{F} = K\mathbf{D}$. The structure of this system is given here for completeness. With respect to a local coordinate system (x_1,x_2,x_3) with x_1 along the bond extension, $\mathbf{D} = (u_{1,p},u_{2,p},u_{3,p},\phi_{1,p},\phi_{2,p},\phi_{3,p},u_{1,q},u_{2,q},u_{3,q},\phi_{1,q},\phi_{2,q},\phi_{3,q})^T$ and $\mathbf{F} = (F_{1,p},F_{2,p},F_{3,p},M_{1,p},M_{2,p},M_{3,p},F_{1,q},F_{2,q},F_{3,q},M_{1,q},M_{2,q},M_{3,q})^T$. The non-zero coefficients on and above the diagonal of K are given by:

$$k_{1,1} = k_{7,7} = -k_{1,7} = \frac{\pi R_\alpha^2 E_b}{L_\beta}, \tag{1a}$$

$$k_{2,2} = k_{3,3} = -k_{8,8} = k_{9,9} = -k_{2,8} = -k_{3,9} = \frac{3\pi R_\beta^4 E_b}{L_\beta}^3, \tag{1b}$$

$$k_{4,4} = k_{10,10} = -k_{4,10} = \frac{\pi R_\beta^4 G_b}{2L_\beta}, \tag{1c}$$

$$k_{5,5} = k_{6,6} = -k_{11,11} = k_{12,12} = 2k_{5,11} = 2k_{6,12} = \frac{\pi R_\beta^4 E_b}{L_\beta}, \tag{1d}$$

$$k_{2,6} = k_{2,12} = -k_{3,5} = -k_{3,11} = k_{5,9} = -k_{6,8} = -k_{8,12} = k_{9,11} = \frac{3\pi R_\beta^4 E_b}{2L_\beta}^2, \tag{1e}$$

where $\beta = 1, 2$, indexes the two types of bonds. The global stiffness of a site-bond model can be assembled from the beam stiffness matrices with appropriate transformations and the linear elastic response determined with any linear solver. We have used ABAQUS (2007) as a solver with its existing provision for beam elements. In this case the modulus of rigidity of the beams is calculated internally from a user defined Poisson's ratio for beams, ν_b, by $G_b = E_b/2(1 + \nu_b)$.

Simulations have been performed with variable parameters R_1/L, R_2/L, G_b/E_b. The ratios R_1/L and R_2/L have been assigned

independently 22 values: 0.01, 0.02, and all the numbers between 0.05 and 1.0 inclusive with step 0.05. Note that the, not included, limiting case, $R_2/L = 0$, corresponds to the simple cubic lattice. Similarly, the, also not included, limiting case, $R_1/L = 0$, corresponds to a lattice formed by the body diagonals only. The ratio G_b/E_b has been assigned independently 24 values in the range 1/3 to 19/3 inclusive with variable step. These correspond to 24 values for Poisson's ratio of the bonds between $\nu_b = 0.5$ and $\nu_b = -0.92$, which will be identifiable in the results.

A site-bond model of a cubic region $(20L,20L,20L)$ defined with respect to a coordinate system (X_1,X_2,X_3), oriented along the three principal directions of the unit cell, has been used for simulations. This represents a cellular lattice with 20 cells in each principal direction. The model has been subjected to uniaxial tension and simple shear external loads to determine the macroscopic modulus of elasticity, Poisson's ratio and shear modulus of rigidity independently. Let (U_1,U_2,U_3) are the displacements of sites with respect to (X_1,X_2,X_3).

The applied boundary conditions for uniaxial tension are: $U_1 = 0$ for sites on $X_1 = 0$; $U_2 = 0$ for sites on $X_2 = 0$; $U_3 = 0$ for sites on $X_3 = 0$; free sites on $X_1 = 20L$; free sites on $X_2 = 20L$; $U_3 = 2L$ for sites on $X_3 = 20L$. This gives an applied macroscopic tensile strain $\varepsilon_t = U_3/20L = 0.1$. The resulting displacements U_1 of sites on plane $X_1 = 20L$ and U_2 of sites on plane $X_2 = 20L$ are averaged to give mean displacements Δ_1 and Δ_2, respectively. The macroscopic Poisson's ratio for tension and compression is determined by $\nu_t = -\Delta_1/L$, or $\nu_t = -\Delta_2/L$. The two values are identical for this model. The macroscopic stress in the direction of the applied macroscopic strain, σ_t, is determined from the reaction forces F_3 at sites on plane $X_3 = 20L$ (or $X_3 = 0$) and the area of this boundary. The macroscopic modulus of elasticity is then calculated by $E = \sigma_t/\varepsilon_t$.

The applied boundary conditions for simple shear are: $U_1 = 0$ for sites on $X_1 = 0$ and on $X_1 = 20L$; free sites on $X_2 = 0$ and on $X_2 = 20L$; $U_2 = U_3 = 0$ for sites on $X_3 = 0$; $U_2 = 2L$ and $U_3 = 0$ for sites on $X_3 = 20L$. This gives an applied macroscopic shear strain $\varepsilon_s = U_2/20L = 0.1$. The macroscopic stress in the direction of the applied macroscopic strain, σ_s, is determined from the reaction forces F_2 at sites on plane $X_3 = 20L$ (or $X_3 = 0$) and the area of this boundary. The macroscopic modulus of rigidity is then calculated by $G = \sigma_s/\varepsilon_s$.

For a given choice of R_1/L, R_2/L, and G_b/E_b, the macroscopic elastic modulus, E, is linearly dependent on the bonds elastic modulus, E_b, which is clear from the structure of the stiffness matrix, Eq. (1). Therefore a fixed E_b has been used throughout the simulations and results are presented for the ratios E/E_b and G/E_b. These can be used to select E_b for obtaining required E and G. A second value of the Poisson's ratio is also calculated from the results for elastic and shear moduli as $\nu_s = E/2G - 1$. The relation $\nu_t = \nu_s$ represents elastic isotropy, while $\nu_t \neq \nu_s$ represents anisotropic behaviour.

4. Results

The parametric studies performed depend on three parameters. Three cases are selected to illustrate their effects on the macroscopic elastic properties of the model. In the first case, the ratio G_b/E_b is fixed at 0.5, that is, the Poisson's ratio of the bonds is $\nu_b = 0$, while the two ratios R_1/L and R_2/L vary within their prescribed intervals. The results for this case are shown in Fig. 3. Plots (a) and (b) show the macroscopic modulus of elasticity, E, and the Poisson's ratio, ν_t, respectively, obtained from the tensile loading of the model. Plot (c) shows the macroscopic modulus of rigidity, G, obtained from the shear loading of the model. In the second case, the ratio R_1/L is fixed at 0.5, while ν_b and R_2/L vary within their prescribed intervals. The results for this case are shown in Fig. 4. In the third case, the ratio R_2/L is fixed at 1.0, while ν_b and R_1/L vary within their prescribed intervals. The results for this case are shown in Fig. 5. The macroscopic elastic properties in the plots (a–c) in Figs. 4 and 5 are same as those in Fig. 3.

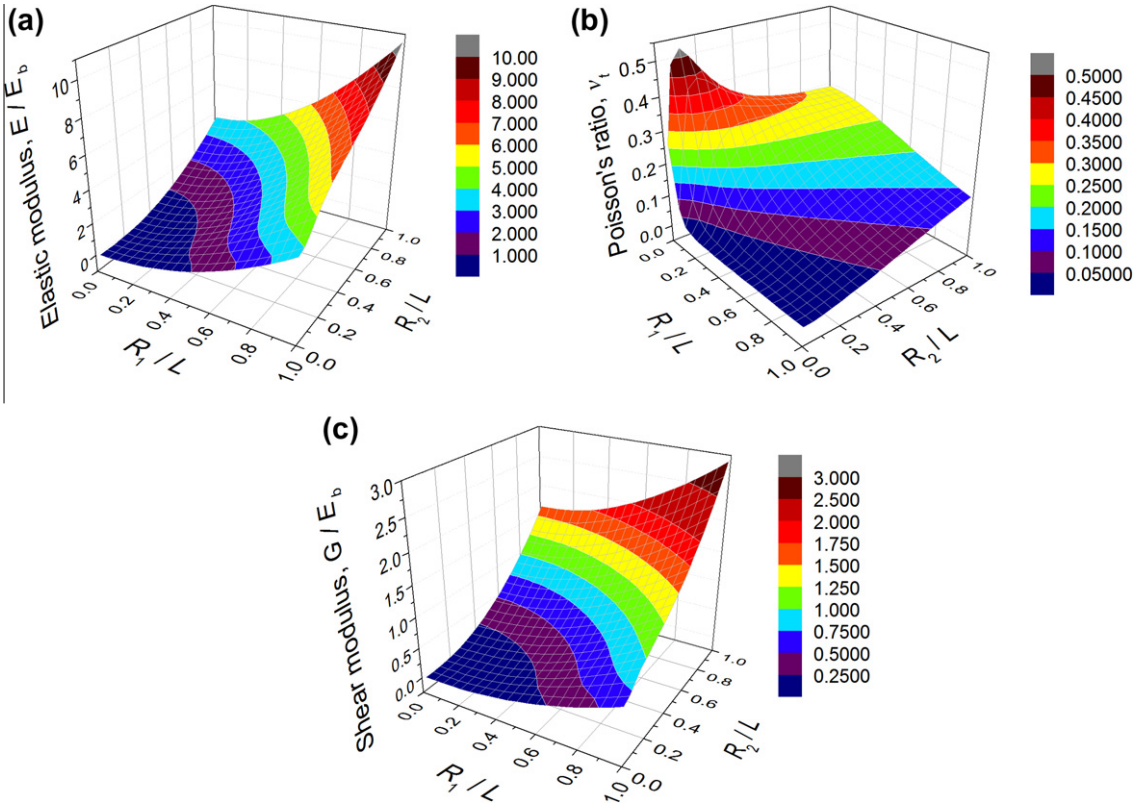

Fig. 3. Macroscopic elastic properties derived with $G_b/E_b = 0.5$ ($\nu_b = 0$) and variable bond radii: modulus of elasticity (a); Poisson's ratio (b); and modulus of rigidity (c).

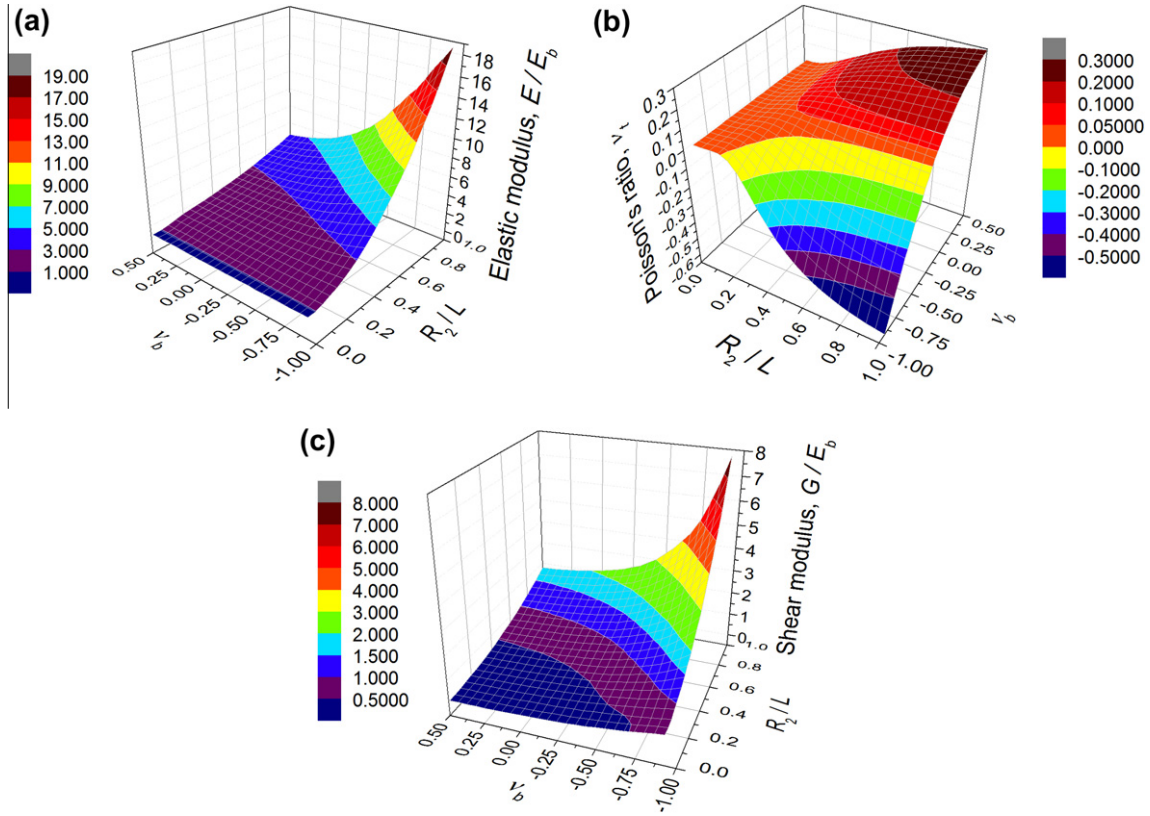

Fig. 4. Macroscopic elastic properties derived with $R_1/L = 0.5$ and variable v_b and R_2/L: modulus of elasticity (a); Poisson's ratio (b); and modulus of rigidity (c).

The results presented in plots (a) of Figs. 3–5 show that increasing bond cross section, equivalent to increasing bond stiffness, and increasing bond shear modulus, or decrease of bond Poisson's ratio, results in increasing macroscopic elastic modulus. Whilst this trend is expected, its analytical treatment may be challenging for the model proposed. The results presented in plots (c) of Figs. 3–5 show a similar trend for the macroscopic shear modulus. Its variation however shows a different complex dependence on the parameters, which is not proportional to the variation of the elastic modulus. The numerical results presented will therefore be useful for calibrating the bond properties of this model.

The results presented in plots (b) of Figs. 3–5 show that elastic materials with Poisson's ratio less than -0.7 and more than 0.5 can be modelled, provided that this is determined as the ratio between the transversal and normal strains from uniaxial tension-compression tests. In fact, for the set of simulations performed, the two limiting values obtained are $v_{t,min} = -0.722$ and $v_{t,max} = 0.564$. Values outside this range can be obtained with higher ratios R_2/R_1 and G_b/E_b than those used here. It is instructive to note that a range of bond properties can be used to obtain a desired macroscopic Poisson's ratio v_t. For any selection of bond cross sections and Poisson's ratio that provide a prescribed v_t, the bond elastic modulus, E_b, can be determined from the results in plots (a) of Figs. 3–5.

It is important to analyse which isotropic elastic materials can be modelled by our site-bond method. These can be extracted from the data as the points where the macroscopic Poisson's ratio, v_t, equals the Poisson's ratio that would be obtained from the elastic and shear moduli, $v_s = E/2G - 1$. An illustration of this process is given in Fig. 6 for the three cases shown in Figs. 3–5. The v_t-surfaces, identical to the plots (b) from Figs. 3–5, are combined with the corresponding v_s-surfaces. The latter are shown in grey, and are only presented in the range where they intersect the v_t-surfaces. The intersection of the two surfaces is a curve, or curves, representing an isotropic elastic material. Some values of the Poisson's ratio at the end points of these curves are depicted for illustration. Fig. 6(a) shows that for $v_b = 0$ the v_s-surface intersects the v_t-surface along a single curve and any isotropic material with $0.26 < v < 0.38$ can be represented. Fig. 6(b) shows that for $R_1/L = 0.5$ the v_s-surface intersects the v_t-surface along two curves, one of which is very short in the neighbourhood of $v = 0.29$. The other intersection shows that any isotropic material with $-0.12 < v < 0.01$ can be represented. Fig. 6(c) shows that for $R_2/L = 1.0$ the v_s-surface intersects the v_t-surface along one curve and any isotropic material with $0.24 < v < 0.29$ can be represented.

Fig. 7 shows the full range of isotropic elastic materials that can be represented by the model. The three plots give the values of the macroscopic Poisson's ratio for variable v_b, R_2/L, and R_1/L, respectively, with solid spheres. Projections of these points on the coordinate planes are also shown with small squares. In Fig. 7(a) the limiting values of the Poisson's ratio are depicted. This shows that there are two regions in which materials can be represented as isotropic by the model.

The first class are materials with $-0.20 < v < 0.02$. Here, the model can represent isotropic cellular foams, which have typically $v < 0$, and rocks which have typically $v \approx 0$. The second class are materials with $0.24 < v < 0.38$. Here, the model can represent as isotropic practically all structural metallic materials, for which the typical range is $0.25 < v < 0.38$. The model can also represent glass and ceramic materials, for which the typical range is $0.24 < v < 0.29$. These results depend on the intervals of the bond parameters used in the analysis. In principle, extending these intervals beyond the current values may increase slightly the regions of available Poisson's ratio for isotropic materials. It should be noted that the assumption of local isotropy, leading to the beam representation of the relative deformations between grains, places

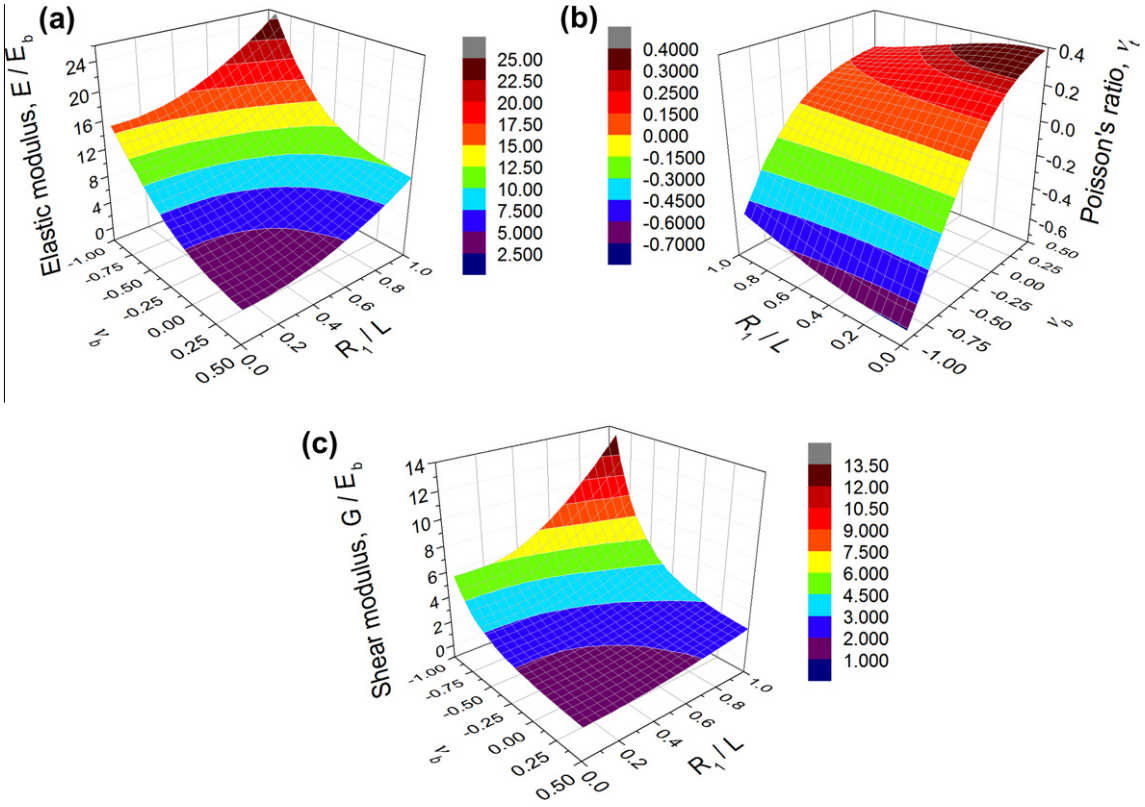

Fig. 5. Macroscopic elastic properties derived with $R_2/L = 1.0$ and variable ν_b and R_1/L: modulus of elasticity (a); Poisson's ratio (b); and modulus of rigidity (c).

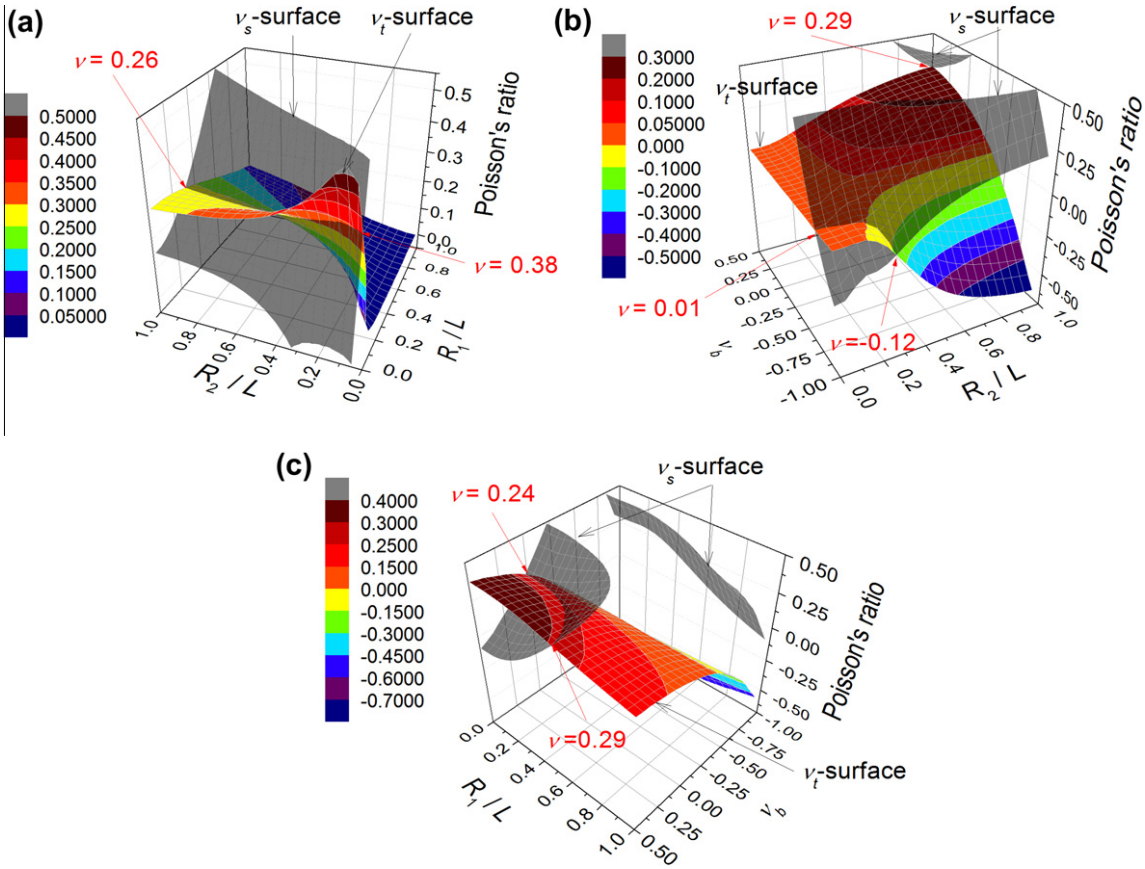

Fig. 6. Macroscopic Poisson's ratios obtained from tensile (coloured surfaces) and shear (grey surfaces) tests for fixed $\nu_b = 0$ (a); fixed $R_1/L = 0.5$ (b); and fixed $R_2/L = 1.0$ (c). The intersection curves of the two surfaces represent homogeneous isotropic materials.

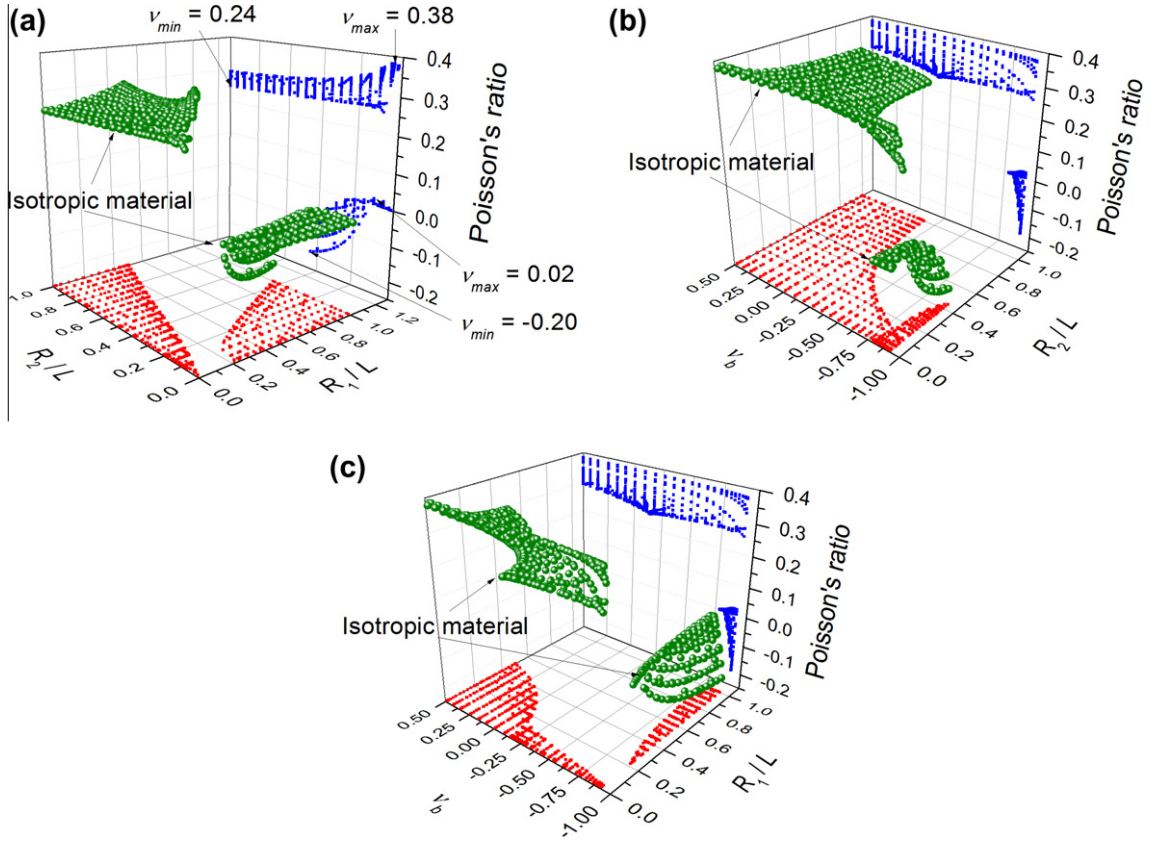

Fig. 7. Values of Poisson's ratio for homogeneous isotropic elastic materials which can be achieved by the model shown in: R_1–R_2 space for all v_b (a); in R_2–v_b space for all R_1 (b); and in R_1–v_b space for all R_2 (c). Projections on the coordinate planes are shown to illustrate the ranges of parameters used. The full range of Poisson's ratios is depicted in plot (a).

some restrictions on the model parameters that can be varied. A more general description can be used, where the tensile and shear behaviours are decoupled, to attempt a wider applicability of the model for isotropic materials if necessary.

An important class of materials that cannot be represented as isotropic are the cement-based materials, for which $0.18 < \nu < 0.22$ is typically reported. These values, however, are obtained experimentally by independent determination of the elastic modulus, E, from tensile or compressive tests, and of the shear modulus, G, from torsion or simple shear tests. A non-destructive way of determining E and G is from measurements of longitudinal and transverse wave velocities. In both cases the reported Poisson's ratio is evaluated assuming isotropic elasticity, $\nu = E/2G - 1$; in our terminology this represents a ν_s value. This can be significantly different from the value determined from tensile or compressive tests as the ratio between transversal and normal strains. Such tests for a number of cement-based materials have shown that $0.24 < \nu_t < 0.33$ (Klink, 1992). This suggests that cementitious materials should not necessarily need to be represented as isotropic. The model allows for tuning the parameters so that the behaviours in tension-compression and shear are sufficiently decoupled to capture the behaviour of this class of materials. We illustrate this by selecting $\nu_t = 0.3$ and studying the set of ν_s that the model can represent.

Fig. 8 shows the ranges of ν_s values that can be obtained for $\nu_t = 0.3$ with various selections of the model parameters. The three plots give the values in the $R_1 - R_2$ space, $R_2 - \nu_b$ space, and $R_1 - \nu_b$ space, respectively, with solid spheres. Projections of these points on the coordinate planes are shown with small squares. In Fig. 8(a) the limiting values of ν_s are depicted. The results demonstrate that if a material with $\nu_t = 0.3$, measured by tension-compression tests, is to be modelled, then our truncated octahedral site bond approach allows for a range of Poisson's ratios measured by shear or torsion tests of $0.13 < \nu_s < 0.5$. This clearly covers the reported range of ν_s for cementitious materials. The process illustrated in Fig. 8 can be repeated for any structural material if the tensile and shear behaviour are found to produce distinctly different Poisson's ratios.

5. Discussion

The approach taken in this work can be regarded as "global" in the sense that the strain energy stored in the entire lattice is compared to the strain energy stored in a continuum with corresponding volume. Moreover a specific representation of the bonds with beams of circular cross-section is used. This was done to illustrate the ability of the newly proposed lattice to represent a wider range of elastic materials than other 3D lattice arrangements that also use beam elements. The approach departs from existing "local" approaches, such as equilibrating the energy in the bonds to the continuum energy stored in a unit cell (Wang and Mora, 2008) or enforcing equilibrium of forces at unit cell level (Cusatis et al., 2011). The reason for this is that the proposed lattice arrangement does not permit a simple closed form solution for the relation between bond properties and continuum elastic constants. In the general case, the behaviour of the two distinct types of bonds, B_1 and B_2, needs to be represented by eight parameters – normal, shear, twisting and bending stiffness for each bond type. With analysis based on unit cell energy equilibrium it can be shown that

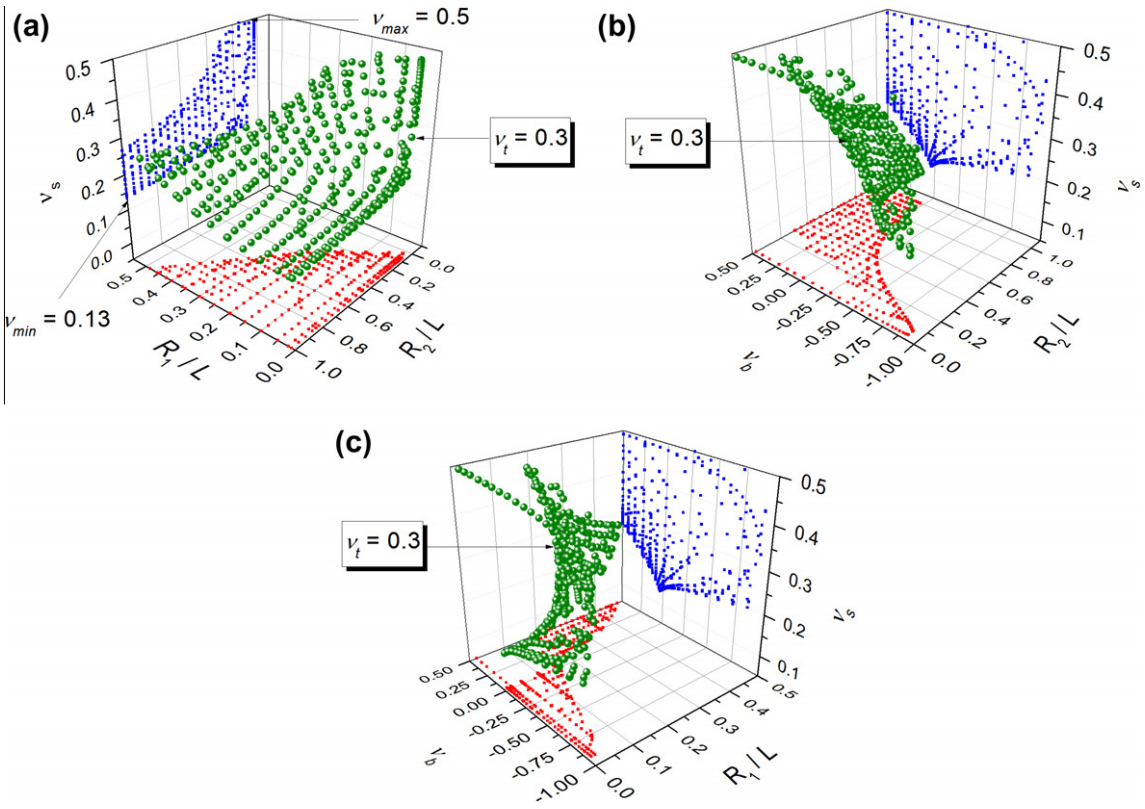

Fig. 8. Values of Poisson's ratio ν_s for materials with $\nu_t = 0.3$ shown in: R_1–R_2 space for all ν_b (a); in R_2–ν_b space for all R_1 (b); and in R_1–ν_b space for all R_2 (c). Projections on the coordinate planes illustrate the ranges of parameters used. The full range of possible ν_s is depicted in plot (a).

the proposed lattice represents a micropolar material with cubic elasticity. This is not surprising as the unit cell of the proposed model is also the Voronoi cell, or the first Brillouin zone, of the face-centred cubic crystals. For the simple case of homogeneous deformation, that of no relative rotations between sites, the three constants of the cubic elasticity can be related to the four normal and shear linear stiffness coefficients of the bonds. This illustrates that the model is over-determined and explains why a given set of macroscopic parameters can be achieved with different combinations of beam properties, as in our results. An analysis of more complex deformation modes involving relative rotations between sites can be used to obtain relations between the linear and the twisting/bending stiffness coefficients. If such analysis is based on deformation energy function dependent on strains only, the classical continuum mechanics used by Wang and Mora (2008), the problem remains over-determined. A possible explanation is that the proposed lattice arrangement is always "micropolar"; the stiffness coefficients of the bonds cannot be uniquely determined from classical strain energy potential. This is a subject of ongoing work and will be reported in a future publication. Nevertheless, the results of this work show that, at the macroscopic scale, the lattice can represent a wide class of materials with isotropic and cubic elasticity, with local micropolar behaviour averaged over the volume.

The presence of micropolar effects at cell level makes it useful for the intended application of the model to the deformation and fracture of solids at the meso-scale (Bazant and Jirasek, 2002). In order to develop the proposed lattice for such studies three immediate areas of future investigation include:

- Derivation of bond properties based on unit cell energy equilibrium and recent developments in micropolar elasticity (Hadjesfandiari and Dargush, 2011).
- Analysis of the relation between micro-crack in a continuum and a micro-crack represented with bond failure in the proposed lattice (see, for example, Yavari et al., 2002).
- Development of inelastic bond model for representing macroscopic elastic–plastic behaviour based on micropolar elasto-plasticity (such as Ristinmaa and Vecchi, 1996).

It has been shown previously that regular lattices lead to bias in fracture paths (Bazant and Jirasek, 2002). This conclusion, however, is made for lattices which are not intrinsically micropolar at the cell level. That is, those lattices with bond properties uniquely related to the constants of classical continuum elasticity. Considering the above discussion, we expect the lattice proposed in this work to overcome this limitation when detailed further analysis is accomplished.

The success of the proposed developments will open two major areas of opportunities. The first is related to problems with mechanically-driven damage, where the micro-cracking is not affected by phenomena other than the local deformation. In this case the micro-failure events are based on a simple criterion, such as failure stress, failure strain or failure strain energy density. Within this class the model can be used to study the effects of material damage on a number of macroscopic material properties. For some macroscopic properties, the solid-phase model will be sufficient: the evolution of the macroscopic stress and strain; changes of thermal conductivity or electrical conductivity of the solid phase. For the former, mechanical solutions will provide the required evolution of the macroscopic stresses and strains for any given boundary conditions. For the later, the discrete model can be solved with appropriate temperature or electric potential boundary conditions after each micro-failure event. In both cases, one can derive a mechanism-based constitutive law for the macroscopic parameter evolution with damage.

For other macroscopic properties, such as diffusivity along grain boundaries or fluid flow through a pore system, a dual site-bond model to supplement the solid-phase model can be constructed. In a dual-phase model the secondary sites are located at the centres of the boundaries of the solid-phase primary model, that is, in the middle of the solid-phase model bonds. These sites represent micro-defects, such as cavities, voids, or pores. The secondary bonds represent links between the micro-defects: perhaps easy pathways for diffusion along boundaries, or throats between pores. There is no requirement that all sites and bonds in the secondary part of the dual-phase model are present initially. This may depend on the size distribution of micro-defects for the particular problem. The problem in the secondary lattice can be solved after each failure event in the primary solid-phase model, so that the evolution of the particular macroscopic property with micro-cracking can be derived to produce a mechanism-based constitutive law.

The second class is related to problems with damage or micro-cracking affected by other phenomena, such as cavity, void, or pore enlargement due to diffusion, corrosion, or internal gas pressure, which may be uncoupled or coupled with mechanical deformation. Within this class of problems a dual-phase model must be used to represent the development of the phenomenon affecting damage. Some examples are:

- Diffusion along the bonds of the secondary model, where the bonds represent grain boundary pathways. The diffusion can be stress-driven taking information from the solid-phase model, concentration-driven from the boundary conditions of the dual model, or a combination of the two. The effects of the diffusion process in terms of micro-defect growth can be communicated back to the solid-phase model to change the bond deformation and failure properties accordingly.
- Corrosion along the bonds and at sites of the secondary model, where bonds represent either grain boundary pathways or throats between pores in a pore system. The corrosion can be driven by electrochemical processes or bacterial attack with appropriate formulation of the dual-phase problem. The effects of the corrosion in terms of micro-defect evolution or internal pore pressure due to gas generation can be communicated back to the solid-phase model for corresponding changes in bond properties.

Multiple parallel models can be developed and linked to a primary solid-phase model if several coupled phenomena need to be accounted for. One attractive opportunity that the proposed approach offers is the study of mechanisms operating at different time scales and their effect on the material performance. Examples would include fatigue crack initiation, delayed hydride fracture, irradiation effects, and the evolution of cementitious or geological materials.

6. Conclusions

- We have conceptualised the meso-scale structure of a wide class of solids with a simple regular cellular lattice based on a truncated octahedron. The key feature of the concept is that the meso-scale behaviour is governed by the microscopic mechanisms of failure.
- We have presented a discrete idealisation of the cellular lattice and have demonstrated that it can be used to describe the elastic behaviour of all materials of practical interest. The discrete system is called a site-bond model of the solid.
- We have shown that a large class of materials can be modelled as macroscopically isotropic; with tension-compression and shear behaviour governed by the same Poisson's ratio. This class includes all structural metallic materials, glasses and ceramics, rocks and porous foams.
- We have shown that materials that are not macroscopically isotropic can also be modelled with tension-compression and shear or torsion behaviour governed by different Poisson's ratios. This class includes cement-based materials.
- We have outlined the most important areas of future research which will develop the site-bond model into a computational tool for investigating deformation and fracture phenomena at meso-scale.

References

ABAQUS, 2007. User's Manual, Version 6.7 ed., Dassault Systemes.

Argon, A.S., Im, J., Safoglu, R., 1975. Cavity formation from inclusions in ductile fracture. Metall. Trans. A 6, 825–837.

Bazant, Z.P., Pang, S.D., 2007. Activation energy based extreme value statistics and size effect in brittle and quasibrittle fracture. J. Mech. Phys. Solids 55, 91–131.

Bazant, Z.P., Jirasek, M., 2002. Nonlocal integral formulations of plasticity and damage: survey of progress. J. Eng. Mech. 128, 1119–1149.

Beremin, F.M., Pineau, A., Mudry, F., Devaux, J.C., D'Escatha, Y., Ledermann, P., 1983. A local criterion for cleavage fracture of a nuclear pressure vessel steel. Metall. Trans. A 14, 2277–2287.

Bordet, S.R., Karstensen, A.D., Knowles, D.M., Wiesner, C.S., 2005. A new statistical local criterion for cleavage fracture in steel. Part I: Model presentation. Eng. Fract. Mech. 72, 435–452.

Chang, C.S., Wang, T.K., Sluys, L.J., Van Mier, J.G.M., 2002. Fracture modeling using a micro structural mechanics approach. I: Theory and formulation. Eng. Fract. Mech. 69, 1941–1958.

Chen, I.W., Argon, A.S., 1981. Diffusive growth of grain-boundary cavities. Acta Metall. 29, 1759–1768.

Chen, J.H., Wang, G.Z., 1992. Study of mechanism of cleavage fracture at low temperature. Metall. Trans. A 23, 509–517.

Cocks, A.C.F., Ashby, M.F., 1982. On creep fracture by void growth. Prog. Mater. Sci. 27, 189–244.

Cundall, P.A., Hart, R.D., 1992. Numerical modelling of discontinua. Eng. Comput. 9, 101–113.

Curry, D.A., Knott, J.F., 1979. Effect of microstructure on cleavage fracture toughness of quenched and tempered steels. Met. Sci. 13, 341–345.

Cusatis, G., Bazant, Z.P., Cedolin, L., 2006. Confinement-shear lattice CSL model for fracture propagation in concrete. Comput. Methods Appl. Mech. Eng. 195, 7154–7171.

Cusatis, G., Pelessone, D., Mencarelli, A., 2011. Lattice discrete particle model (LDPM) for failure behaviour of concrete. I: Theory. Cement Concr. Compos. 33, 881–890.

De Borst, R., 2002. Fracture in quasi-brittle materials: a review of continuum damage-based approaches. Eng. Fract. Mech. 69, 95–112.

Griffiths, D.V., Mustoe, G.G.W., 2001. Modelling of elastic continua using a grillage of structural elements based on discrete element concepts. Int. J. Numer. Methods Eng. 50, 1759–1775.

Gurson, A.L., 1977. Continuum theory of ductile rupture by void nucleation and growth. Part 1: Yield criteria and flow rules for porous ductile media. J. Eng. Mater. Technol. – Trans. ASME 99, 2–15.

Hadjesfandiari, A.R., Dargush, G.F., 2011. Couple stress theory for solids. Int. J. Solids Struct. 48, 2496–2510.

Hofstetter, G., Meschke, G., 2011. Numerical Modelling of Concrete Cracking, first ed. Springer, Berlin.

Hoover, W.C., Hoover, C.C., 2001. Spam-based recipes for continuum simulations. Comput. Sci. Eng. 3, 78–79.

Jain, S., Budiansky, N.D., Hudson, J.L., Scully, J.R., 2010. Surface spreading of intergranular corrosion on stainless steels. Corros. Sci. 52, 873–885.

Jing, L., 2003. A review of techniques, advances and outstanding issues in numerical modelling for rock mechanics and rock engineering. Int. J. Rock Mech. Mining Sci. 40, 283–353.

Jivkov, A.P., Lidbury, D.P.G., James, P., 2011. Assessment of local approach methods for predicting end-of-life toughness of RPV steels. In: Proceedings of the ASME 2011 Pressure Vessels and Piping Division Conference, Paper 57546.

Jivkov, A.P., Stevens, N.P.C., Marrow, T.J., 2006. A three-dimensional computational model for intergranular cracking. Comput. Mater. Sci. 38, 442–453.

Klink, S.A., 1992. Cement and the elastic constants of concrete. Cement Concr. Res. 22, 761–768.

Kumar, S., Kurtz, S.K., Banavar, J.R., Sharma, M.G., 1992. Properties of a three-dimensional Poisson–Voronoi tesselation: a Monte Carlo study. J. Stat. Phys. 67, 523–551.

Lo, K.H., Shek, C.H., Lai, J.K.L., 2009. Recent developments in stainless steels. Mater. Sci. Eng. R 65, 39–104.

Monaghan, J.J., 2005. Smoothed particle hydrodynamics. Rep. Prog. Phys. 68, 1703–1759.

Mudry, F., 1987. A local approach to cleavage fracture. Nucl. Eng. Des. 105, 65–76.

Rice, J.R., Tracey, D.M., 1969. On the ductile enlargement of voids in triaxial stress fields. J. Mech. Phys. Solids 17, 201–217.

Ristinmaa, M., Vecchi, M., 1996. Use of couple-stress theory in elasto-plasticity. Comput. Methods Appl. Mech. Eng. 136, 205–224.
Rousselier, G., 1987. Ductile fracture models and their potential in local approach of fracture. Nucl. Eng. Des. 105, 97–111.
Ruggieri, C., Dodds Jr, R.H., 1996. A transferability model for brittle fracture including constraint and ductile tearing effects: a probabilistic approach. Int. J. Fract. 79, 309–340.
Schlangen, E., 2008. Crack development in concrete. Part 2: Modelling of fracture process. Key Eng. Mater. 385–387, 73–76.
Schlangen, E., van Mier, J.G.M., 1992. Experimental and numerical analysis of micromechanisms of fracture of cement-based composites. Cement Concr. Compos. 14, 105–118.
Silling, S.A., 2000. Reformulation of elasticity theory for discontinuities and long-range forces. J. Mech. Phys. Solids 48, 175–209.
Sukumar, N., Moes, N., Moran, B., Belytschko, T., 2000. Extended finite element method for three-dimensional crack modelling. Int. J. Numer. Methods Eng. 48, 1549–1570.
Taylor, S.W., Jaffe, P.R., 1990. Biofilm growth and the related changes in the physical properties of a porous medium. 1: Experimental investigation. Water Resour. Res. 26, 2153–2159.
Thomason, P.F., 1985. A three-dimensional model for ductile fracture by the growth and coalescence of microvoids. Acta Metall. 33, 1087–1095.
Tvergaard, V., Needleman, A., 1984. Analysis of the cup-cone fracture in a round tensile bar. Acta Metall. 32, 157–169.
Wang, Y., Mora, P., 2008. Macroscopic elastic properties of regular lattices. J. Mech. Phys. Solids 56, 3459–3474.
Xu, X.P., Needleman, A., 1993. Void nucleation by inclusion debonding in a crystal matrix. Model. Simul. Mater. Sci. Eng. 1, 111–132.
Yavari, A., Sarkani, S., Moyer Jr., E.T., 2002. On fractal cracks in micropolar elastic solids. J. Appl. Mech. 69, 45–54.